Catalysis Today 148 (2009) 134–139

Contents lists available at ScienceDirect

Catalysis Today

journal homepage: www.elsevier.com/locate/cattod

Pore geometry influence on the deactivation behavior of Ni-based catalysts for simultaneous production of hydrogen and nanocarbon

J. Salmones [a], J.A. Wang [a], M.A. Valenzuela [a,*], E. Sánchez [a], A. Garcia [b]

[a] Laboratorio de Catalísis y Materiales, ESIQIE-Instituto Politécnico Nacional, Zacatenco, C.P. 07738, México D.F., Mexico
[b] UPIICSA, Instituto Politécnico Nacional, Te 950 Col. Granjas-México, 08400 México D.F., Mexico

ARTICLE INFO

Article history:
Available online 1 May 2009

Keywords:
Methane decomposition
Ni/Mg–Al–O
Hydrogen production
Pore geometry

ABSTRACT

Pore geometry of Ni-containing Mg–Al–O mixed oxide catalysts could be controlled by varying the Ni content in the synthesis. Low Ni content may lead to the catalysts having mesopores with shape cylinder and narrow pore size distribution; high Ni content results in the catalyst having pores with shape ink-bottle and a wide pore size distribution. In methane decomposition to produce hydrogen and nanocarbon, the 50 wt.% Ni/Mg–Al–O catalyst was rapidly deactivated after 2 h of reaction; however, the catalysts with 15 and 25 wt.% of Ni showed much longer lifetime, which can be explained by assuming a new modal related to pore geometry of the catalysts.

© 2009 Elsevier B.V. All rights reserved.

1. Introduction

The demand for hydrogen is ever increasing due to a variety of utilization in chemical processing, electronics, food processing, metal manufacturing and fuel cells [1]. Steam reforming (SR), partial oxidation or autothermal reforming of hydrocarbons and alcohols have been the conventional methods to produce hydrogen [2]. A general disadvantage of these processes is the formation of carbon monoxide and carbon dioxide, which are difficult to separate from hydrogen [3]. Furthermore, for certain applications, like in fuel cell technology, carbon monoxide has to be removed from hydrogen in order to prevent the electro-catalyst from poisoning [4]. Recently, the catalytic decomposition of methane (CDM) has received extensive attention as a potential process for the production of high-purity hydrogen [5–16]. The reaction is moderately endothermic and the energy required for the production of 1 mol hydrogen (45.1 kJ mol^{-1} at 800 °C) is less than that required for SR of methane (48.0 kJ mol^{-1}). Unlike the SR process, the CDM process does not include water gas shift reaction, selective oxidation of remained CO and pressure-swing adsorption stages, which considerably simplifies the process and reduces the operation cost [7,17]. The produced carbon may be used as the substitutes of carbon black, fibers, graphite, composites, carbon fillers in tires and plastics or be used as catalyst support [18]. Deposited carbon also can be oxidized with H_2O and O_2 into CO, synthesis gas and CO_2. The CDM into hydrogen and carbon followed by catalyst regeneration in oxidative atmosphere can be carried out in a cyclic manner in the same reactor [8,19] or by stepwise steam of carbon formed on the catalyst [20].

The most studied catalysts for the CDM are nickel supported on: SiO_2, SiO_2–Al_2O_3, SiO_2–MgO, SiO_2–CeO_2, TiO_2, graphite, ZrO_2, Al_2O_3, MgO, $ZnAl_2O_4$, CeO_2, TiO_2, La_2O_3, Y_2O_3, oxidized diamond, among others [5–16]. Other metals such as Fe, Pt, Pd, Cr, Ru, Mo or W on different supports have been successfully tested in the CDM [8,21,22]. Unfortunately, rapid deactivation of Ni-based catalyst takes place at temperatures above 500 °C, leading to a low yield of hydrogen [23]. The catalyst deactivation occurs when the metallic particles are encapsulated by non-reactive carbon compounds [24]. It is, therefore, a major challenge to develop a catalytic system that sustains its activity at high temperatures and drastic regeneration processes to avoid metal sintering. The nature of support usually shows important effect on the catalytic activity of the catalysts, as it is well known that the change of the structure or electronic state of the metal active species is correlated with the interaction between metals and support. The surface area and thermal stability of the catalysts support are intensely investigated; however, less attention is paid on the study of the pore geometrical effect of the support. For example, to date, in the reaction of CDM, contribution of the pore geometry of support to the catalytic stability of the Ni-containing catalysts has not been reported yet. Furthermore, the addition of MgO to the Ni-based catalysts induces the formation of Ni–Mg–O solid solutions and could confer specific features to the Ni active sites [25]. Certainly, the stabilization of small sized Ni crystallites with MgO causes a

* Corresponding author. Tel.: +52 55 5729 6000x55112; fax: +52 55 5586 2728.
E-mail address: mavalenz@ipn.mx (M.A. Valenzuela).

0920-5861/$ – see front matter © 2009 Elsevier B.V. All rights reserved.
doi:10.1016/j.cattod.2009.03.005

strong metal–support interaction which could improve the activity and resistance to deactivation [26].

In this work, three different Ni/Mg–Al–O catalysts prepared from hydrotalcite-like precursor used in the CDM to produce hydrogen and nanocarbon were investigated. The influence of the Ni content on the pore geometry of the catalysts and thus on the catalytic activity and stability at severe reaction conditions was explored.

2. Experimental

2.1. Catalysts preparation

A mixture solution of metal salts was prepared by adding 21.83 g of $Mg(NO_3)_2{\cdot}6H_2O$ and 15 g of $Al(NO_3)_3{\cdot}H_2O$ into 500 ml deionized water, respectively; the second solution was obtained by dissolving 14 g of NaOH and 3.3 g of Na_2CO_3 in 100 ml of water. Then, the second solution was added, drop by drop, into the first solution to obtain a suspension mixture. The pH of the mixture was kept between 9.5 and 10 by adjusting the addition of the base solution. The precipitates were kept in suspension under stirring at room temperature for 2 h. To obtain Ni-containing catalyst, 100 ml of $Ni(NO_3)_2$ solution with different concentrations was added into the above suspension at a rate 60 drops/min with stirring. The amount of $Ni(NO_3)_2$ in the solution depends on the desired Ni content in the catalysts. After washed and filtered by several times, the resultant material was dried at 120 °C for 10 h. Three samples containing 15, 25, and 50 wt.% Ni were obtained with the similar synthetic procedure described above. These samples were calcined at 873 K for 4 h in a static air atmosphere; it causes an attack on the hydrotalcite structure and in turn forms oxide (MgO, NiO) and spinel-like ($Mg_xNi_{1-x}Al_2O_4$) phases. Before the catalytic evaluation, the catalysts were reduced with hydrogen at 500 °C for 2 h. These catalysts are refereed as Ni/Mg–Al–O.

2.2. Catalysts characterization

The power X-ray diffraction (XRD) data of the materials were collected at room temperature in a Siemens D-5000 diffractometer with Cu Kα radiation. The diffraction patterns were identified by a comparison with those included in the JCPDS data base (Joint Committee of Powder Diffractions Standards).

The textural properties of the catalysts were measured using N_2 adsorption–desorption isotherms on a Micromeritics Digisorb ASAP 2100. Before the measurement, the sample was evacuated at 300 °C under vacuum condition. The surface area was calculated using the Brunauer–Emmett–Teller (BET) method. The pore size distribution was calculated by using the Barrett–Joyner–Halenda (BJH) model.

Temperature-programmed reduction (TPR) experiments were performed in a Micromeritics TPD/TPR–2900 apparatus using a mixture of 5 vol.% hydrogen in argon with a heating rate of 5 °C/min from room temperature to 800 °C. Before the TPR experiment, the sample was pretreated at 400 °C for 1 h using dried air with a flow rate 50 ml/min.

The carbon formation and metal particle on the deactivated catalysts were studied by using high resolution transmission electron microscopy in a JEOL 4000 EX electron microscope.

2.3. Catalytic activity and stability measurements

Catalytic performances of the Ni/Mg–Al–O catalysts were evaluated in a stainless steel fixed bed reactor (10 mm i.d., 500 mm in length) at atmospheric pressure and temperature 580 °C. Catalyst loading was 0.1 g and a total flow rate of 100 ml/min was used. The space velocity GHSV was 60,000 h^{-1}. The feed stream was a mixture of high-purity methane diluted in argon (20 mol% of methane). The inlet and outlet effluents were monitored by an on-line gas chromatograph (GC) analyzer with a PE-Molsieve capillary column, using a thermal conduct detector (TCD) for hydrogen analysis and a flame ionization detector (FID) for methane analysis.

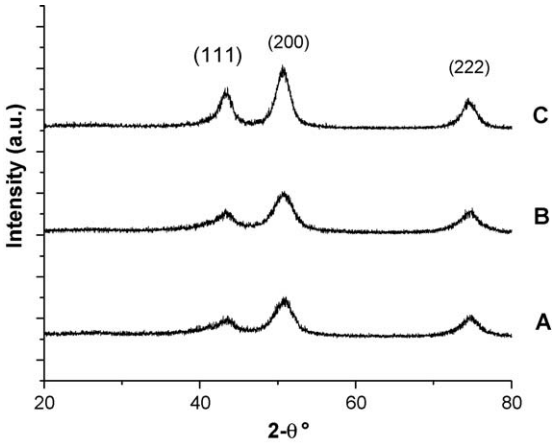

Fig. 1. XRD diffraction patterns for reduced catalysts. (A) 15 wt.% Ni/Mg–Al–O; (B) 25 wt.% Ni/Mg–Al–O; (C) 50 wt.% Ni/Mg–Al–O.

3. Results and discussion

The catalysts calcined at 600 °C consist mainly of NiO and $(Mg_xNi_{1-x})Al_2O_4$ spinel-like phases. No hydrotalcite phase was detected by XRD analysis because it is thermal unstable and might be decomposed into spinel-like phase after calcination. After reduction at 580 °C with hydrogen, the NiO phase transformed into metallic Ni crystals and the Ni contained into the spinel-like phase was also converted to Ni crystals, as shown in Fig. 1. The three diffraction peaks at $2\theta = 44.5°$, 51.8° and 76.4° correspond to (1 1 1), (2 0 0) and (2 2 2) planes of the metallic crystals, respectively. The average size of Ni crystals obtained from the X-ray diffraction data is approximately 20 nm for the 15 wt.% Ni, 33 nm for the 25 wt.% Ni and 45 nm for the 50 wt.% Ni catalysts (Table 1).

Textural data of the catalysts are reported in Table 1. All catalysts show moderate BET specific areas between 275 and 120 m^2/g. It gradually diminishes with increasing of the Ni loading. When the Ni content increases to 50 wt.%, its surface area drops to less than half of that of the 15 wt.% Ni/Mg–Al–O catalyst.

Fig. 2(A–C) shows the profiles of N_2 adsorption–desorption isotherms. The hysteresis loops of the samples A and B are associated with the typical mesopore systems in type IV with pore shape cylinder. The profile C consists of almost vertical and nearly parallel adsorption and desorption branches, it shows a hysteresis loop of type II, indicating that the catalyst C contains pores with shape ink-bottle.

Fig. 3(A–C) shows the pore size distributions of the catalysts. The average mesopore diameter of the samples A and B is between 3 and 9 nm. The catalyst with 15 wt.% Ni presents a uniformed

Table 1
Ni content, Ni particle size and textural properties of the catalysts.

Catalysts	Ni content (wt.%)	Average Ni particle size (nm)	Pore volume (cm^3/g)	Surface area (m^2/g)
A	15	20	0.255	274
B	25	33	0.304	230
C	50	45	0.480	120

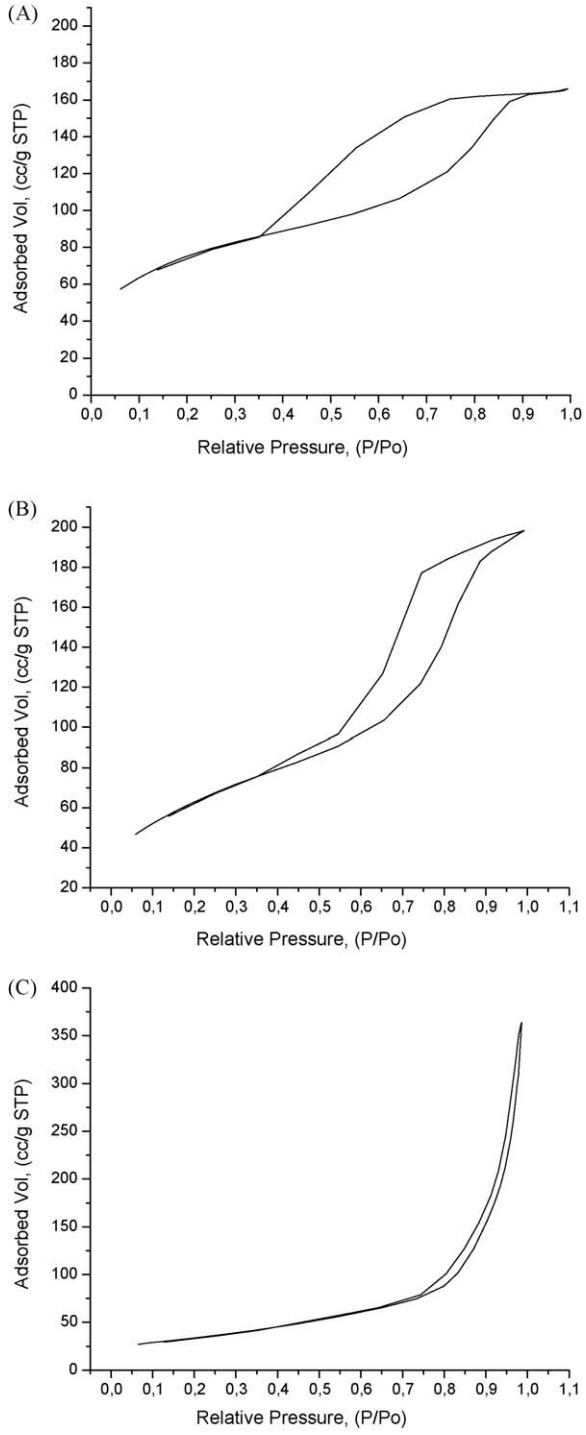

Fig. 2. Profiles of N_2 adsorption–desorption isotherms of the different catalysts. (A) 15 wt.% Ni/Mg–Al–O; (B) 25 wt.% Ni/Mg–Al–O; (C) 50 wt.% Ni/Mg–Al–O.

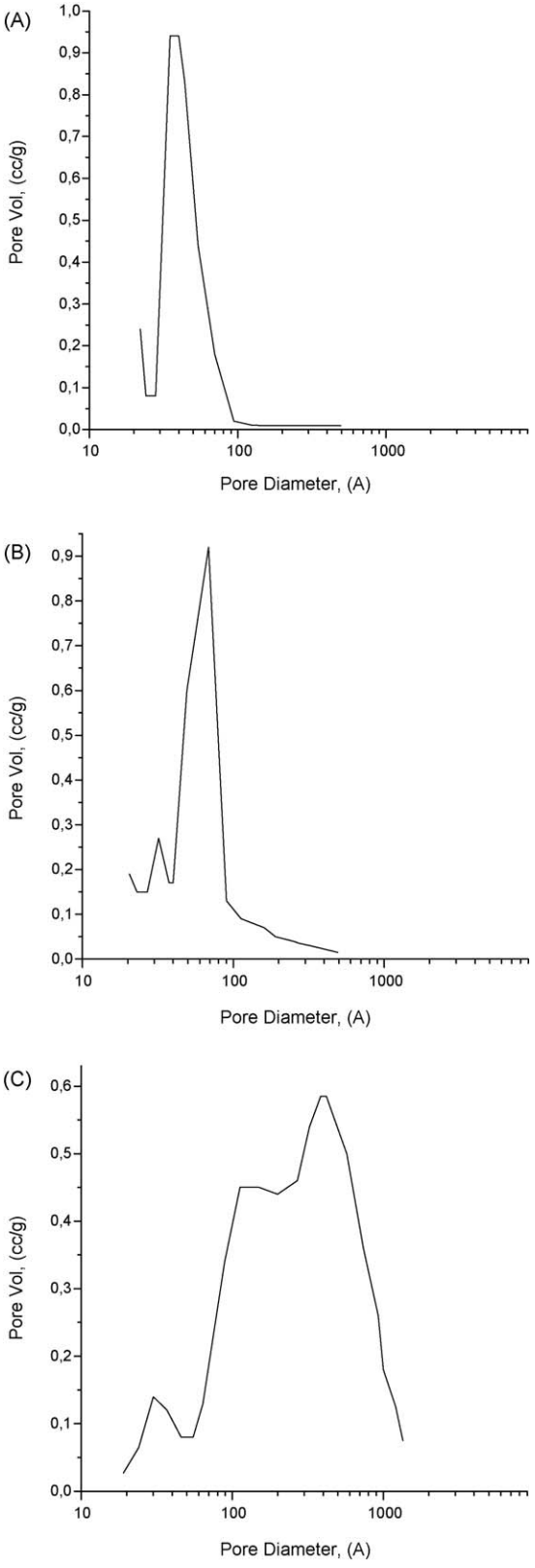

Fig. 3. Pore diameter distributions of the different catalysts: (A) 15 wt.% Ni/Mg–Al–O; (B) 25 wt.% Ni/Mg–Al–O; (C) 50 wt.% Ni/Mg–Al–O.

monomodal pore size distribution centred at 3.7 nm, and a bimodal pore size distribution is formed for the 25 wt.% Ni/Mg–Al–O: one small peak centred at 3.3 nm and one mayor peak between 3 and 9 nm with a maximum 5.1 nm. The catalyst with 50 wt.% Ni exhibits a rather wide pore size distribution between 2 and 100 nm. It shows tri-modal distribution which consists of three peak maxima at around 3, 13 and 50 nm, respectively. Above results indicate that the Ni content significantly impacts not only the Ni crystallite size but also the pore shape and pore diameter distribution of the catalysts.

To obtain information about the dependence of surface oxygen species or active sites, TPR experiments were performed; the TPR profiles were plotted in Fig. 4. In general, TPR can provide semi-quantitative descriptions of domain sizes and monolayer

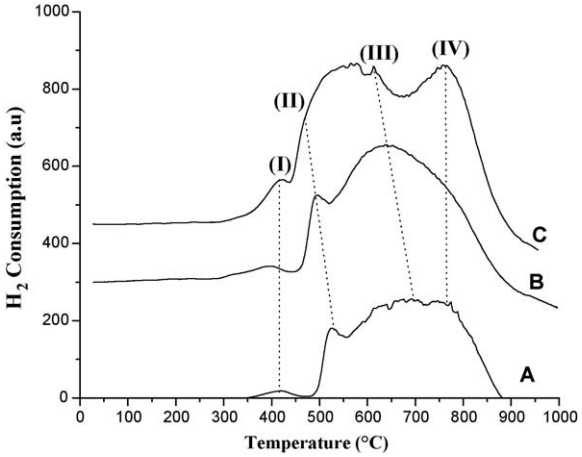

Fig. 4. TPR profiles of the calcined catalysts: (A) 15 wt.% Ni/Mg–Al–O; (B) 25 wt.% Ni/Mg–Al–O; (C) 50 wt.% Ni/Mg–Al–O.

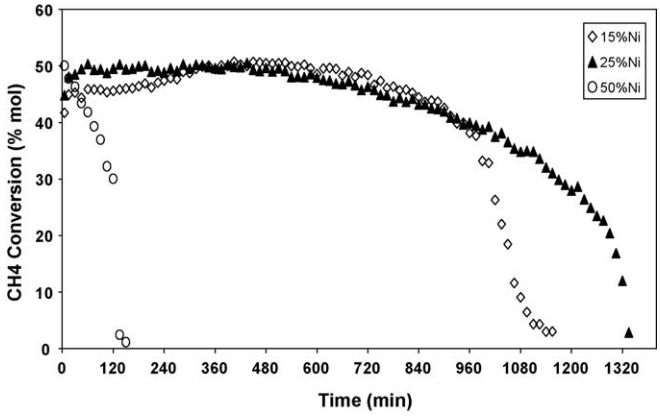

Fig. 5. Evaluation of catalytic activity stability at 580 °C, atmospheric pressure and 20 mol% methane in Ar. (A) 15 wt.% Ni/Mg–Al–O; (B) 25 wt.% Ni/Mg–Al–O; (C) 50 wt.% Ni/Mg–Al–O.

capacities for surface oxides. Dispersed oxides tend to be reduced at higher temperatures than bulk crystallites because of strong M–O bonds with oxide surface and a lack of metal oxide nearest neighbours to share the reduced charge. TPR methods are often useful indicators of the onset of bulk metal oxide crystallite formation, caused by a progression from isolated species to two-dimensional structures and three-dimensional clusters. The area under the TPR curve is directly related to the H_2 consumption during reduction, and knowing the amount of consumed hydrogen and the amount of reducible cations, thus the original oxidation state of the cation can be determined.

In the temperature range of 350–900 °C, these catalysts were characterized by one small peak (I) around 410 °C followed by a large and broad peak that begins at 440 °C and exceeds beyond at 900 °C, the latter is not well resolved and it can be deconvoluted to three overlapping components II, III and IV. These results indicate the existences of several kinds of oxygen species or several forms of oxides on the samples that exhibit different reduction behaviors.

In the low temperature at 410 °C, there is a small peak I in the TPR profile, which is mostly due to the inserted hydroxyls in the structure reacting with H_2. In these mixed oxide samples, it is possible to retain a small quantity of hydroxyls into the structure, which is difficult to be removed off in the oxidation condition, however, it is possible for these species to react with hydrogen in the TPR condition. The second peak II is probably due to the reduction of NiO with large particles that had weak interaction with the support. While, the peak III is attributed to the reduction of highly dispersed NiO in small particles size. As the Ni content increases, the temperature corresponding to the peak maximum of the peak III shifts to low temperature range, indicating that the interaction of the NiO with the support becomes weak. As discussed above, the reduction of the isolated NiO particles takes place at higher temperature because of the lack of the metal oxide nearest neighbours to share the reduced charge. At low Ni concentration, there are not enough NiO neighbours with Ni–O–Ni linkage in these small domains, most of the NiO should form isolated oxide; as the NiO amount increases, NiO particle diameter grows and shares with more neighbours, which lead to the reduction occurring at relatively low temperature. Addition to it, the peak area of the peak III gradually increases with increasing of the Ni amount, which can be easily understood because of more hydrogen consumption for the reduction of more NiO particles.

It is seen that the position of the peak IV is independent of Ni content; it remains its position maximum unchanged in the three samples, indicating that it is a reduction of the same form of Ni–O species. With respect to the results of XRD analysis, some of the Ni^{2+} replace Mg^{2+} ion in the lattice cell reacting with Al^{3+} to form a mixed spinel compound (Mg, Ni)Al_xO_y and the fact that the spinel type material is rather difficult to be reduced, therefore, the peak IV in the TPR profile may correlate with reduction of strong Ni–O–Al bond in the (Mg, Ni)Al_xO_y compound.

The catalytic activity of our catalysts for CH_4 decomposition was continuously evaluated for 22 h, as shown in Fig. 5. Methane conversion over 50 wt.% Ni/Mg–Al–O catalyst rapidly decreased from around 50% at beginning to 5% after 2 h of reaction, indicating a rapid deactivation of the catalyst. However, the other two catalysts show high catalytic stability. During 15 h of reaction, the methane conversion remains almost unchanged. Particularly, the 25 wt.% Ni/Mg–Al–O catalyst still remains good catalytic activity after 20 h of reaction.

TEM observations of the deactivated catalysts indicate high carbon content (Fig. 6). Carbon nanotubes with approximately 30–40 nm diameter and several hundred nanometers in length are observed in the TEM image. The black dots belong to nickel particles. The Ni particles are located on the tip of the carbon nanotubes.

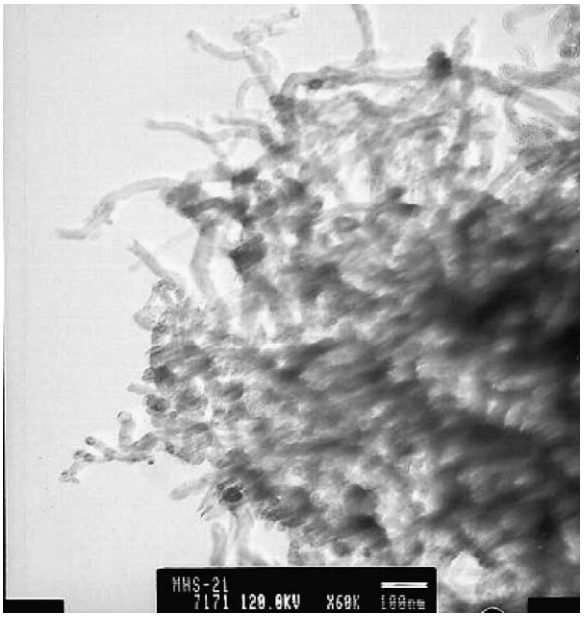

Fig. 6. A high resolution TEM image of the deactivated catalyst (A: 15 wt.% Ni/Mg–Al–O).

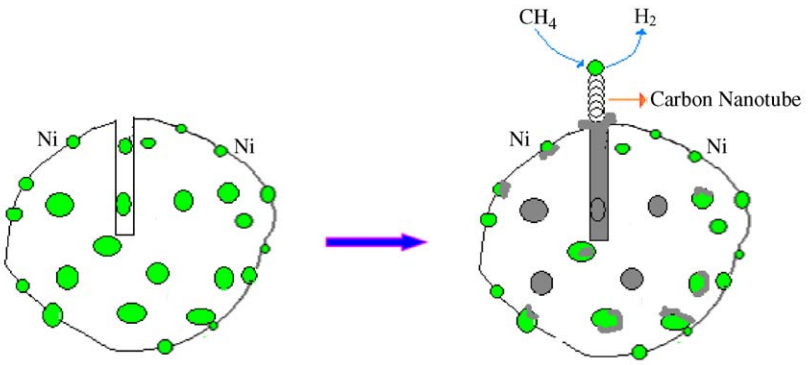

Before and after deactivation of 15 wt % Ni/Mg-Al-O and 25 wt% Ni/Mg-Al-O catalysts

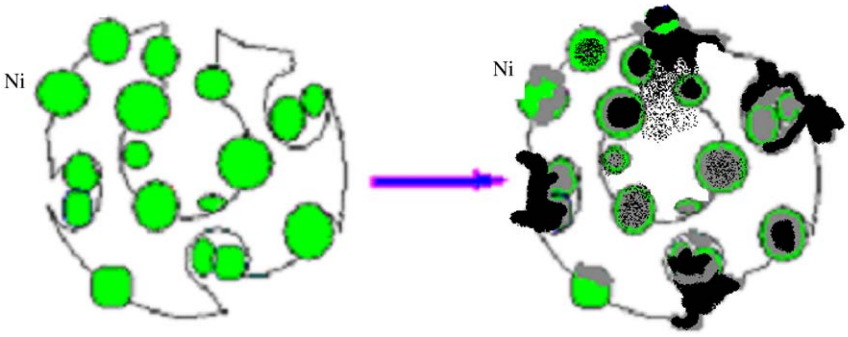

Before and after deactivation of 50 wt% Ni/Mg-Al-O catalyst

Scheme 1. Catalyst deactivation models and carbon nanotubes formation.

On the basis of results obtained, an assumption is described in Scheme 1 to explain the different deactivation behaviors of the catalysts. For the 50 wt.% Ni/Mg–Al–O catalyst, due to its wide pore diameter distribution and large pores, it is possible that the metallic Ni particles are mostly located inside the pores. As the methane decomposition reaction takes place, the produced non-reactive carbon covered on the surface of the larger Ni particles. Because most of the Ni are located inside the pore mouths, as the reaction proceeds, the pore mouths are full with carbon materials until they are completely blocked, thus most of the active phase Ni are locked inside the ink-bottle-like pores, this may be mainly responsible for rapid deactivation within 2 h of reaction.

For the 15 wt.% Ni/Mg–A–O and 25 wt.% Ni/Mg–Al–O catalysts, due to their small cylinder shape pores and very narrow pore size distribution, the Ni particles are mostly located on the pore openings along with some Ni crystals with small diameter were inside the pore mouths. Produced carbon located around the Ni particles and they may support the Ni on the tip of the carbon nanotubes as they grow, this carbon growth mode effectively avoids the active Ni phases from rapid encapsulation by carbon, which greatly prolongs the catalyst lifetime.

4. Conclusions

On the basis of the above results described we conclude as follows:

- It has been possible to obtain Ni-containing Mg–Al–O mixed oxides catalysts with controllable pore geometry by varying the Ni content. Low Ni content may lead to mono- or bimodal pore size distribution with pore shape cylinder, and high Ni content, i.e., 50 wt.%, may result in wide pore size distribution with pore shape ink-bottle.
- In CDM reaction, rapid deactivation was observed on the 50 wt.%/Mg–Al–O catalyst within 2 h of reaction; however, over the 15 and 25 wt.%/Mg–Al–O catalysts, after 15 h of reaction, the catalytic activity remained almost unchanged. The rapid deactivation of the catalyst with high Ni content is assumed to be related to low accessibility of the active Ni particles locating inside the ink-bottle pores which are easily embedded by the produced carbon materials in a short period of reaction. On the contrary, the Ni particles in the catalysts with low Ni content are mainly located on the pore openings and situated on the tip of the produced carbon nanotubes, remaining its high accessibility for continuous reaction and thus prolonging their lifetime.

Acknowledgments

This work has been developed under support of research projects: CGPI 20090210 and CONACyT Nos. 44118 and 51007 and project of ICyTDF-2008.

References

[1] T.V. Choudhary, E. Aksoylu, D.W. Goodman, Catal. Rev. 45 (2003) 151.
[2] Y. Jamal, M.-L. Wyszynski, Int. J. Hydrogen Energy 19 (1994) 557.
[3] J.R. Rostrup-Nielsen, Catal. Rev. 46 (2004) 247.
[4] L.D. Andrews, J. Power Sources 61 (1996) 113.
[5] K. Otsuka, S. Kobayashi, S. Takenaka, J. Catal. 200 (2001) 4.
[6] N.Z. Muradov, T.N. Veziroğlu, Int. J. Hydrogen Energy 30 (2005) 225.
[7] N.Z. Muradov, Energy & Fuels 12 (1998) 41.
[8] T. Zhang, M.D. Amiridis, Appl. Catal. A: Gen. 167 (1998) 161.
[9] Y. Li, J. Chen, Y. Qin, L. Chang, Energy & Fuels 14 (2000) 1188.
[10] S. Takenaka, H. Ogihara, I. Yamanaka, K. Otsuka, Appl. Catal. A: Gen. 217 (2001) 101.
[11] N. Shah, D. Panjala, G.P. Huffman, Energy & Fuels 15 (2001) 1528.

[12] M.A. Valenzuela, O. González, I. Córdova, S. Flores, J.A. Wang, Chem. Eng. Trans. 4 (2004) 61.
[13] K. Otsuka, S. Takenaka, Catal. Surv. Asia 8 (2004) 77.
[14] H. Wang, R.T.K. Baker, J. Phys. Chem. B 108 (2004) 20273.
[15] R.A. Couttenye, M.H. De Vila, S.L. Suib, J. Catal. 233 (2005) 317.
[16] O. González, M.A. Valenzuela, J.A. Wang, Mater. Res. Soc. Symp. Proc. 885E (2006) 233.
[17] M. Steinberg, H.C. Cheng, Int. J. Hydrogen Energy 14 (1989) 797.
[18] A. Venugopal, S. Naveen Kumar, J. Ashok, D. Hari Prasad, V. Durga Kumari, K.B.S. Prasad, M. Subrahmanyam, Int. J. Hydrogen Energy 32 (2007) 1782.
[19] T.V. Choudhary, D.W. Goodman, J. Catal. 192 (2000) 316.
[20] V.R. Choudhary, S. Banerjee, A.M. Rajput, Appl. Catal. A: Gen. 234 (2002) 259.
[21] K. Nakagawa, M. Nishitani, T. Ando, Int. J. Hydrogen Energy 30 (2005) 201.
[22] N. Muradov, Catal. Commun. 2 (2001) 89.
[23] B. Monnerat, L. Kiwi-Minsker, A. Renken, Chem. Eng. Sci. 56 (2001) 633.
[24] T.V. Choudhary, C. Sivadinarayana, C.C. Chusuei, A. Klinghoffer, D.W. Goodman, J. Catal. 199 (2001) 9.
[25] G. Italiano, C. Espro, F. Arena, F. Frusteri, A. Parmaliana, Catal. Lett. 124 (2008) 7.
[26] N. Latorre, J.I. Villacampa, T. Ubieto, E. Romeo, C. Royo, A. Borgna, A. Monzòn, Top. Catal. 51 (2008) 158.